

## Stability of dendritic arrays

James A. Warren

*Department of Physics, University of California, Santa Barbara, California 93106*

J. S. Langer

*Institute for Theoretical Physics, University of California, Santa Barbara, California 93106*

(Received 5 March 1990)

We propose an approximate method for studying steady-state properties and linear stability of the dendritic arrays that are formed in directional solidification of alloys. Our analysis is valid at high growth rates where the primary spacing between dendrites is larger than the velocity-dependent solutal diffusion length. We compute a neutral stability boundary and find that, in the situations where we expect our results to be valid, the experimental data of Somboonsuk, Mason, and Trivedi [Metall. Trans. A **15A**, 967 (1984)] lie in the stable region, well away from the boundary.

### I. INTRODUCTION

One of the original metallurgical motives for the study of dendritic crystal growth was the need to predict and control the microstructures of cast alloys.<sup>1</sup> Now that we have what appears to be a reliable theory of the behavior of individual dendrites,<sup>2-4</sup> it should be possible to answer questions about the collective properties of the large dendritic arrays that occur in many practical casting processes. The work to be described here is part of an effort to bring the modern developments in dendrite theory back to the applications with which it started.

The leading edge of the solidification front can be visualized as an array of dendritic tips advancing, in parallel to one another, into a supersaturated melt. The partially solidified region between the tips of the dendrites and the fully solidified material is called the mushy zone, and it is within this zone that the microstructural properties of the alloy are established. In particular, the dendritic pattern in the mushy zone determines the pattern of solute segregation in the cast solid; the latter pattern, in turn, determines the mechanical properties of the material and its behavior under further processing.

Figure 1 is a schematic illustration of the front of the mushy zone. One feature of this pattern that is of special interest for metallurgical applications is the average spacing between the primary dendrites, denoted here by  $\lambda_1$ . It is also important, especially if one is looking ahead toward accurate numerical simulations of casting processes, to know the temperature and solute concentrations at the leading edge of the zone and thus to know the parameters which determine the shape of the primary dendrites, the initial spacing of the secondary sidebranches, and the volume fraction of the solid and the associated solute concentration as functions of distance behind this edge. These are all interrelated quantities.

The primary spacing problem has long been of interest within the metallurgical community, and various attempts to solve it have appeared in the literature. We do not find any of these attempts entirely convincing, largely

because each of them—in one way or another—has tried to find a unique primary spacing  $\lambda_1$  that depends only on the current growth conditions and not on the way those conditions were achieved, and each has done this by making some *ad hoc* assumption about the shapes of the dendrites. For example, Kurz and Fisher<sup>5</sup> assumed that the envelope of primary dendritic structure is an ellipse whose semiminor axis is  $\lambda_1$  and whose semimajor axis is the thickness of the mushy zone. Hunt,<sup>6</sup> on the other hand, used a spherical approximation for the front of the dendrite and coupled this with the assumption (due to Schiel) that the solute concentration in the melt, in the bulk of the mushy zone, varies only in the direction of growth.

In what follows, we propose to take a different point of view. First, we are going to argue that there is no unique primary spacing at fixed growth conditions—that, in general, there exists a continuous range (possibly very narrow) of physically allowable states (i.e., primary spacings), and that the selected state depends upon the sequence of events by which the system has been set into motion. This notion of no sharp selection is consistent with a growing body of theoretical and experimental evidence regarding cellular spacings in directional solidification,<sup>7,8</sup> and we see no reason to suspect that this situation will change abruptly when the cells become dendrites.

Second, given the assumption of a band of allowed spacings, we do not need to look for additional *ad hoc* selection condition, and can focus, instead, on the dynamic properties of arbitrarily chosen arrays. In particular, we shall examine the morphological stability of the leading edge of the mushy zone in the hope that the dynamic information obtained in this way will provide clues about history-dependent pattern selection. More specifically, our scheme for the present investigation is to test experimental data to see whether measured spacings are consistent with the stability criterion and, if so, how far they might be from the limit of stability. Such a theoretical test can be meaningful, however, only if the experiments have been carried out in such a way that all

of the system parameters required by the theory are independently determined—there should be no adjustable constants. So far as we know, the only experiment that fits this criterion is that of Somboonsuk, Mason, and Trivedi,<sup>9</sup> who measured primary spacings of two-dimensional arrays of dendrites growing in dilute solutions of acetone in succinonitrile. As we shall see, their results are quite interesting from a theoretical point of view.

## II. A MODEL FOR DENDRITIC DIRECTIONAL SOLIDIFICATION

The basic model of directional solidification to be used here is described in Ref. 10. Hydrodynamic degrees of freedom are neglected; all transport is assumed to be diffusive. In addition, the latent heat of fusion is assumed to be sufficiently small and thermal conductivities of the liquid and solid sufficiently large and close to one another that the temperature throughout the system can be taken to be

$$T(z) = T_0 + Gz, \quad (2.1)$$

independent of the position or shape of the solidification front. As shown in Fig. 1,  $z$  measures displacement parallel to the direction of motion in a frame moving at velocity  $v$ . The temperature  $T_0$  is the melting temperature of the pure material, and  $G$  is the thermal gradient which is taken to be a constant under control of the experimentalist. Note that, because the tips of the dendrites must be undercooled, this choice of position for  $z=0$  means that the entire solidification front will be in the region  $z < 0$ .

It is convenient, but not essential for the kind of analysis to be described here, to assume that the alloy is sufficiently dilute that we can make linear approximations for the liquidus and solidus in the equilibrium phase diagram. (That approximation is accurate for the alloys used in the experiments of Somboonsuk *et al.*) Let  $m$  and  $m'$  be, respectively, the liquidus and solidus slopes ( $dT/dc$ ). The symbol  $c$  denotes the concentration of the solute; and the ratio  $m/m' = K < 1$  is the partition coefficient. The initial concentration of the liquid, that is, the concentration infinitely far ahead of the solidification front, is  $c_\infty$ .

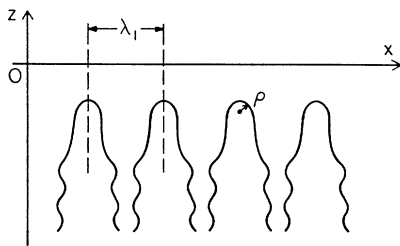


FIG. 1. Schematic illustration of dendritic tips at the front of the mushy zone. The point  $z=0$ , at which the temperature is equal to the melting temperature of the pure material, is moving upwards (in the positive  $z$  direction) at speed  $v$ .

The starting point for this analysis is the diffusion equation for the solute concentration  $c(\mathbf{r}, t)$  as a function of position  $\mathbf{r} = (r_1, z)$  and time  $t$  in the moving frame

$$\frac{\partial c}{\partial t} - v \frac{\partial c}{\partial z} - D \nabla^2 c = \sum_{i=0}^{\infty} \mathcal{S}_i(\mathbf{r}, t). \quad (2.2)$$

Here  $D$  is the solutal diffusion constant in the fluid. This equation is valid, of course, only in the fluid phase; no diffusion occurs in the solid. The symbol  $\mathcal{S}_i$  denotes the source strength associated with the  $i$ th dendrite, that is, the rate at which the solute is being rejected into the fluid at positions  $\mathbf{r}$  along the solidification front. Equation (2.2) has the formal solution

$$c(\mathbf{r}, t) = c_\infty + \sum_i \int d\mathbf{r}' \int_{-\infty}^t dt' \mathcal{G}(\mathbf{r}, t | \mathbf{r}', t') \mathcal{S}_i(\mathbf{r}', t'), \quad (2.3)$$

where  $\mathcal{G}$  is the Green's function for the operator on the left-hand side of (2.2). Strictly speaking,  $\mathcal{G}$  is a very complicated function because of the one-sided boundary conditions at the solidification front. For present purposes—in anticipation of the approximations to be introduced shortly—it needs not be written out explicitly.

Our strategy is to use Eq. (2.3) to write an equation of motion, not for the entire solidification front, but only for the positions  $z_i(t)$  of the tips of the dendrites. To do this, we need to make a number of serious assumptions, several of which are very specific to dendritic—as opposed to cellular—situations. These are the following.

(i) Quasistationarity. The explicit time dependence of  $\mathcal{S}_i$  in (2.3) may be neglected because the motion of the solidification front relative to the moving frame is slow compared to the rate at which the diffusion field adjusts to changes in the front. The source strength  $\mathcal{S}_i$  still depends implicitly on the time, however, because it is a function of the instantaneous growth rate  $v_i$  and the radius of curvature of the tip  $\rho_i$ .

(ii) Slender, three-dimensional dendrites. The tip of each dendrite is assumed to be well separated both from all other tips and from the walls of the container. That is, the tip radii  $\rho_i$  are all much smaller than the interdendritic spacing  $\lambda_1$  and the smallest dimension, say  $W$ , of the channel in which the solidification is taking place.

(iii) Local equilibrium. The concentration  $c_i$  at the position  $z_i$  of the  $i$ th tip is fixed by the liquidus on the phase diagram, that is,

$$c_i = -\frac{G}{m} z_i. \quad (2.4)$$

Note that we are omitting the Gibbs-Thomson correction here. Capillarity plays a role only in the next of these assumptions.

(iv) Solvability. The instantaneous growth rate  $v_i$  of the  $i$ th tip is determined by a solvability condition of the form

$$\frac{2Dd_0}{v_i \rho_i^2} = \sigma^*. \quad (2.5)$$

Here  $d_0$  is the capillary length

$$d_0 = \frac{\gamma T_0}{(\Delta c_i)Lm} = -\frac{\gamma T_0}{(1-K)LGz_i}, \quad (2.6)$$

where  $L$  is the latent heat per unit volume and  $\Delta c_i = -(1-K)Gz_i/m$  is the jump in equilibrium concentration of solute between the solid and liquid phases at a temperature  $T_0 + Gz_i$  [see Ref. 10, Eq. (3.5) and the associated footnote].

In writing (2.5) we implicitly assume that  $\sigma^*$  is independent of the solutal Péclet number

$$p_i = \frac{\rho_i v_i}{2D}. \quad (2.7)$$

For the well-separated dendrites of interest to us  $p_i$  will be small, of order  $10^{-2}$  or less, and the limit  $p_i \rightarrow 0$  almost certainly is accurate enough for our purposes. A more serious assumption, especially for growth conditions near the cell-to-dendrite transition, is that the solvability condition does not depend on the spacing  $\lambda_1$ . In general, we must expect that when  $\lambda_1$  is less than the diffusion length  $l \equiv 2D/v$ , the dendritic tips will interact so strongly with each other that their shapes will be deformed and, therefore, the solvability mechanism for velocity selection will be significantly altered. In short, we are making the strong assumption that the properties of any dendritic tip on our array are the same as those of an isolated dendrite growing slowly in a homogeneous melt.

For pure succinonitrile solidifying under conditions of thermal control, where the symmetric model with equal thermal diffusivities in both the solid and liquid phases is appropriate,  $\sigma^*$  is known to be about 0.02. The value of  $\sigma^*$  should be twice as large for the one-sided model as it is for the symmetric model, thus, we shall assume  $\sigma^* \approx 0.04$  for succinonitrile with solutal control.

The next step is to evaluate each term in Eq. (2.3) at the tip of, say, the  $i$ th dendrite. Consider first the contribution to the sum in (2.3) from the  $j$ th dendrite with  $j \neq i$ . Denote this contribution by the symbol  $\delta c_{ij}$ . According to assumption (ii), the region near the tip of this dendrite should look like a one dimensional source of solute when observed from distances of order  $\lambda_1 \gg \rho_j$ . Thus with quasistationarity (i) and the assumption of a paraboloidal tip  $z = -r_\perp^2/2\rho_j$ ,

$$\begin{aligned} \mathcal{S}_j(\mathbf{r}, t) d\mathbf{r} &\rightarrow \mathcal{S}_j(z) \delta^2(\mathbf{r}_\perp - \mathbf{r}_\perp) dz, \\ \mathcal{S}_j(z) &\approx [\Delta c_j(z)] v_j 2\pi r_\perp \left| \frac{dr_\perp}{dz} \right| dz \\ &= [\Delta c_j(z)] v_j 2\pi \rho_j dz, \end{aligned} \quad (2.8)$$

where  $z$  is the position along the axis of the  $j$ th dendrite and  $r_\perp$  is the radial distance away from this axis. In this three-dimensional situation,  $\mathcal{S}_j$  depends on  $z$  only through the factor  $\Delta c_j(z) = -(1-K)Gz/m$  plus the condition that  $\mathcal{S}_j$  vanishes for  $z > z_j$ .

It seems reasonable when considering the contributions from distant line sources to neglect perturbations of the diffusion field caused by neighboring or intervening dendrites and, accordingly, to approximate  $\mathcal{G}$  in (2.3) by  $\mathcal{G}_F$ ,

the Green's function for diffusion in free space. The formula that is needed is

$$\int_0^\infty dt \mathcal{G}_F(\mathbf{r}, t | 0, 0) = \frac{1}{4\pi D |\mathbf{r}|} \exp\left[-\frac{z + |\mathbf{r}|}{l}\right] \equiv \Gamma(|\mathbf{r}|, z), \quad (2.9)$$

where  $l = 2D/v$  is the diffusion length. The resulting contribution to the sum in (2.3) is

$$\delta c_{ij} \approx \int_{-\infty}^{z_j} dz' \Gamma[d_{ij}(z'), z_i - z'] \Delta c(z') 2\pi \rho_j v_j, \quad (2.10)$$

where

$$d_{ij}(z') = [\lambda_{ij}^2 + (z_i - z')^2]^{1/2}, \quad (2.11)$$

and  $\lambda_{ij}$  is the distance, in the plane perpendicular to the growth direction, between the  $i$ th and  $j$ th dendrites. Carrying out the integration in (2.10), we find

$$\begin{aligned} \delta c_{ij} &= \frac{G p_j (1-K)}{m} \\ &\times \left[ \frac{l}{2} \left[ 1 - \frac{\lambda_{ij}^2}{l d_{ij}} \right] \exp\left[-\frac{d_{ij}}{2l}\right] \right. \\ &\quad \left. - \left[ z_i - \frac{\lambda_{ij}^2}{2l} \right] E_1\left[\frac{d_{ij}}{l}\right] \right], \end{aligned} \quad (2.12)$$

where  $d_{ij} \equiv d_{ij}(z_j)$  in (2.11) and  $E_1$  is the exponential integral

$$E_1(x) = \int_x^\infty \frac{e^{-t}}{t} dt. \quad (2.13)$$

Approximating  $\mathcal{S}_i$  by a line source is not appropriate for the term  $\delta c_{ii}$ , where the point  $\mathbf{r}$  at which  $c(\mathbf{r})$  is being evaluated is the tip of the paraboloidal surface from which solute is being rejected. In this case, we must replace  $\lambda_{ij}^2$  in (2.11) by  $r_\perp^2 = 2\rho_i(z_i - z')$  to obtain the correct distance between a source at  $z'$ ,  $r_\perp(z')$ , and the tip. Once again, the integration can be carried out without further approximation, and the result is

$$\begin{aligned} \delta c_{ii} &= \frac{G(1-K)p_i}{m} \\ &\times \left[ \frac{l}{2} \left[ 1 + \frac{\rho_i}{l} \right] - \left[ z_i + \rho_i + \frac{\rho_i^2}{2l} \right] E_1\left[\frac{\rho_i}{l}\right] \right]. \end{aligned} \quad (2.14)$$

This is the familiar Ivantsov relation generalized to the case of a free solutally controlled dendrite growing in the direction of a temperature gradient. Note, however, that  $\rho_i/l$  is not quite the same as the Péclet number  $p_i$  because the diffusion length  $l = 2D/v$  is computed at the fixed growth speed  $v$  and not at the instantaneous growth rate  $v_i$  of the  $i$ th tip.

Combining the formal solution of the diffusion equation (2.3) evaluated at the tip of the  $i$ th dendrite, with the boundary condition (2.4) and the specific results (2.12) and (2.14), we find

$$\frac{z_i - z_\infty}{(1-K)} = \rho_i e^{\rho_i/l} E_1 \left[ \frac{\rho_i}{l} \right] \left[ z_i + \rho_i + \frac{\rho_i^2}{2l} \right] - \frac{\rho_i}{2} \left[ 1 + \frac{\rho_i}{l} \right] + \sum_{i \neq j} p_j \left[ \left[ z_i - \frac{\lambda_{ij}^2}{2l} \right] E_1 \left[ \frac{d_{ij}}{l} \right] + \frac{l}{2} \left[ 1 - \frac{\lambda_{ij}^2}{ld_{ij}} \right] \exp \left[ -\frac{d_{ij}}{l} \right] \right]. \tag{2.15}$$

Here

$$z_\infty = -\frac{mc_\infty}{G} \tag{2.16}$$

is the position along the  $z$  axis at which solidification might first occur and, thus, is a first approximation for the leading edge of the mushy zone and a reasonable reference point from which to measure the tip positions  $z_i$ .

Equation (2.15) provides us with one set of relations between the quantities  $z_i$  and  $\rho_i$  for fixed relative positions of the dendrites, that is, for fixed separations  $\lambda_{ij}$ . Note that the velocities  $v_i$  which occur in the Péclet numbers  $p_i$  are related to  $z_i$  via

$$v_i = v + \frac{dz_i}{dt}. \tag{2.17}$$

Therefore the solvability condition (2.5) is the second set of relations needed for a mathematically complete set of equations of motion for this system. As expected, these equations make sense—at least formally—for any geometrical arrangement of the dendrites; the spacings  $\lambda_{ij}$  are parameters which describe a continuous family of growth patterns. The existence of a family is actually a necessary consequence of the point of view we have taken

here. We know that the combination of a solvability condition (2.5) plus Ivantsov relation (2.14) is sufficient to determine uniquely the growth rates and tip radii of isolated dendrites. The full equation (2.15) reduces to (2.14) in the limit of large spacings  $\lambda_{ij}$  because the coupling terms (for  $i \neq j$ ) vanish in this limit. Thus we clearly have a family of—not necessarily stable—steady-state solutions at large separations; and we must expect that family to persist at least for weakly interacting arrays of dendrites.

As outlined in the Introduction, our procedure from this point is to compute steady-state solutions of (2.5) and (2.15), and then to examine their stability. This procedure is completely straightforward. In the remainder of this section, we shall simply write down the relevant equations and then, in Sec. III, we shall use these formulas to interpret the data of Somboonsuk, Mason, and Trivedi.<sup>9</sup>

The steady-state versions of (2.5) and (2.15) are obtained by assuming a completely uniform, flat, front of the mushy zone:  $v_i = v$ ,  $z_i \equiv z \equiv -|z|$ ,  $\rho_i \equiv \rho$ , and  $p_i = \rho/l = \rho v/2D \equiv p$ . We then have

$$\frac{2D\gamma T_0}{(1-K)LGv\rho^2|z|} = \sigma^*, \tag{2.18}$$

and

$$\frac{|z| - |z_\infty|}{(1-K)} = p e^p E_1(p) \left[ |z| - \rho - \frac{\rho p}{2} \right] + \frac{\rho}{2} (1+p) + p \sum_{i \neq j} \left[ \left[ |z| + \frac{\lambda_{ij}^2}{2l} \right] E_1 \left[ \frac{\lambda_{ij}}{l} \right] + \frac{l}{2} \left[ \frac{\lambda_{ij}}{l} - 1 \right] \exp \left[ -\frac{\lambda_{ij}}{l} \right] \right]. \tag{2.19}$$

To study linear stability, we assume that all small departures from steady state grow (or decay) with an amplification rate  $\omega$ . For example,

$$z_i - z = \delta z_i e^{\omega t}, \quad v_i - v = \omega \delta z_i e^{\omega t}, \dots \tag{2.20}$$

Then from the solvability condition, we find

$$\delta p_i = \frac{p}{2} \left[ \frac{1}{|z|} + \frac{\omega}{v} \right] \delta z_i, \tag{2.21}$$

and

$$\delta \rho_i = \frac{\rho}{2} \left[ \frac{1}{|z|} - \frac{\omega}{v} \right] \delta z_i. \tag{2.22}$$

We also have

$$\delta E_1 \left[ \frac{\rho_i}{l} \right] = -e^p \frac{\delta \rho_i}{\rho}, \tag{2.23}$$

$$\delta E_1 \left[ \frac{d_{ij}}{l} \right] = -\frac{\exp(-\lambda_{ij}/l)}{\lambda_{ij}} (\delta z_i - \delta z_j), \tag{2.24}$$

and

$$\delta \exp \left[ -\frac{d_{ij}}{l} \right] = -\frac{\exp(-\lambda_{ij}/l)}{l} (\delta z_i - \delta z_j). \tag{2.25}$$

The linearized version of (2.15) can now be written in the form of an eigenvalue equation for  $\omega$ :

$$\omega \sum_j A_{ij} \delta z_j = \sum_j B_{ij} \delta z_j, \quad (2.26)$$

$$A_{ij} = A^{(0)} \delta_{ij} + (1 - \delta_{ij}) A_{ij}^{(1)},$$

$$B_{ij} = B^{(0)} \delta_{ij} + (1 - \delta_{ij}) B_{ij}^{(1)}, \quad (2.27)$$

where

with

$$A^{(0)} = \frac{p}{2v} \left[ e^p E_1(p) \left[ |z| (1-p) + \frac{lp^2}{2} (3+p) \right] + |z| + \frac{l}{2} (1-2p-p^2) \right], \quad (2.28)$$

$$A_{ij}^{(1)} = \frac{p}{2v} \left[ \left[ |z| + \frac{\lambda_{ij}}{2l} \right] E_1 \left[ \frac{\lambda_{ij}}{l} \right] + \frac{1}{2} (l - \lambda_{ij}) \exp \left[ -\frac{\lambda_{ij}}{l} \right] \right], \quad (2.29)$$

$$B^{(0)} = -\frac{1}{(1-K)} + pe^p E_1(p) \left[ \frac{1}{2} (1-p) + \frac{pl}{2|z|} \left[ 2 + \frac{5p}{2} + \frac{p^2}{2} \right] \right] \\ + \frac{p}{2} - \frac{pl}{4|z|} (1+4p+p^2) + p \sum_{i \neq j} \left[ E_1 \left[ \frac{\lambda_{ij}}{l} \right] + \frac{|z|}{\lambda_{ij}} \exp \left[ -\frac{\lambda_{ij}}{l} \right] \right], \quad (2.30)$$

$$B_{ij}^{(1)} = -\frac{p}{2|z|} \left[ |z| + \frac{\lambda_{ij}^2}{2l} \right] E_1 \left[ \frac{\lambda_{ij}}{l} \right] + p \left[ \frac{1}{4|z|} (\lambda_{ij} - l) - \frac{|z|}{\lambda_{ij}} \right] \exp \left[ -\frac{\lambda_{ij}}{l} \right]. \quad (2.31)$$

Finally, if the array of dendrites is periodic, (2.26) can be solved by Fourier transformation, yielding a dispersion relation for  $\omega$  as a function of wave vector  $\mathbf{q}$ :

$$\omega(\mathbf{q}) = \frac{\hat{B}(\mathbf{q})}{\hat{A}(\mathbf{q})}, \quad (2.32)$$

where

$$\hat{A}(\mathbf{q}) = \sum_j A_{ij} \exp(-i\mathbf{q} \cdot \Lambda_{ij}); \quad \hat{B}(\mathbf{q}) = \sum_j B_{ij} \exp(-i\mathbf{q} \cdot \Lambda_{ij}), \quad (2.33)$$

and the  $\Lambda_{ij}$  are the lattice vectors of length  $\lambda_{ij}$ .

### III. COMPARISONS WITH EXPERIMENT

In the experiments of Somboonsuk, Mason, and Trivedi,<sup>9</sup> a 5% molar solution of acetone in succinonitrile was directionally solidified in the gap between parallel glass plates. The system was accelerated abruptly to speed  $v$  so that the initially flat interface underwent a series of instabilities and settled, ultimately, into a dendritic array. Measurements were made of the average spac-

ing  $\lambda_1$ , and also the average tip radii and secondary spacings of the sidebranches, for sequences of different values of speed  $v$  and temperature gradient  $G$ . Values of the physical constants relevant to this system are shown in Table I.

These experiments were carried out in such a way that the spacing between the plates, denoted here by  $W$ , was generally much smaller than the primary spacing  $\lambda_1$  but much larger than the tip radius  $\rho$ . Thus the pattern gen-

TABLE I. Physical properties of succinonitrile and succinonitrile-acetone solutions [from Somboonsuk, Mason, and Trivedi (Ref. 9)].

Succinonitrile	
Melting point	331.24 K
Entropy of fusion	11.21 J/mol K
Density of solid	$1.016 \times 10^3$ kg/m <sup>3</sup>
Density of liquid	$0.970 \times 10^3$ kg/m <sup>3</sup>
Thermal conductivity of solid	0.224 J/m s K
Thermal conductivity of liquid	0.223 J/m s K
Surface energy	$8.95 \times 10^{-3}$ J/m <sup>2</sup>
Succinonitrile-Acetone	
Diffusion coefficient	$1.27 \times 10^{-5}$ cm <sup>2</sup> /s
Liquidus slope	-2.22 K/mol % acetone
Equilibrium partition ratio	0.10

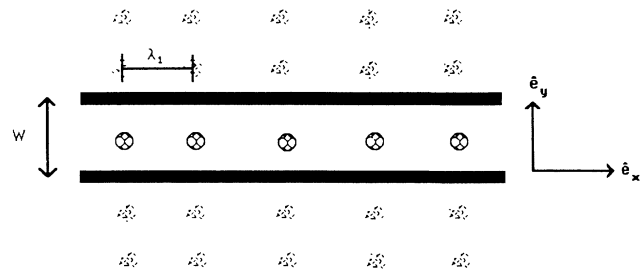


FIG. 2. Transverse section of dendrites growing in a narrow gap between parallel plates. The growth direction is perpendicular to the plane of the paper. The plates are indicated by dark bars. The physical dendritic tips (between the plates) and their images (outside) form a two-dimensional array of spacing  $\lambda_1$  in the  $x$  direction and  $W$  in the  $y$  direction.

TABLE II. Experimental data of Somboonsuk, Mason, and Trivedi (Ref. 9) (first five columns) and theoretical predictions of steady-state tip radii (last column).

$V$ ( $\mu\text{m/s}$ )	$G$ (K/cm)	$\lambda_1$ ( $\mu\text{m}$ )	$\lambda_1/l$	$\rho_{\text{exp}}(\mu\text{m})$	$\rho_{\text{theor}}(\mu\text{m})$
1.17	67.0	472.0	0.22	23.0	6.019
2.15	65.0	377.0	0.32	13.6	7.428
3.97	67.0	328.0	0.51	10.3	7.563
3.97	67.0	324.0	0.51	9.8	7.570
10.7	66.7	240.5	1.01	6.2	5.479
10.7	67.0	240.0	1.01	6.3	5.479
25.5	66.7	174.2	1.75	4.0	3.603
65.6	65.6	125.2	3.23	2.3	2.216
100	67.0	96.8	3.81	1.8,2.2	1.777
65.3	29.6	182.0,180.0	4.68,4.63	2.86	2.222,2.222
65.8	42.4	144.0,156.0	3.73,4.04	2.56	2.213,2.213
65.9	52.0	144.0,142.0	3.74,3.68	2.30	2.213,2.213
65.0	65.6	125.0,134.6	3.20,3.44	2.6,2.31	2.227,2.227
64.3	77.0	116.7,123.0	2.95,3.11	2.3,2.5	2.240,2.240
10.6	29.9	370.0	1.54	5.25	5.530
10.6	41.0	332.5	1.39	5.73	5.517
10.6	46.7	262.0,268.0	1.09,1.12	5.27	5.512,5.512
10.5	63.7	240.5,250.0	0.99,1.03	5.4	5.523,5.526
10.8	77.0	209.9,202.0	0.98,0.86	5.73	5.454,5.455

erated was a two-dimensional array of dendrites whose tips were effectively three dimensional. The zero-flux boundary condition at the plates is achieved mathematically by extending this two-dimensional array periodically into a third dimension perpendicular to the plates. A transverse section of the resulting system of dendrites and their images is shown in Fig. 2. To perform the sums in the various formulas in Sec. II, we write  $\Lambda_{ij} = n_{ij}\lambda_1\mathbf{e}_x + m_{ij}W\mathbf{e}_y$ , where  $n_{ij}$  and  $m_{ij}$  are integers and  $\mathbf{e}_x$  and  $\mathbf{e}_y$  are unit vectors as shown in the figure. For this situation, the wave vector  $\mathbf{q}$  introduced in (2.32) and (2.33) must be chosen to be in the  $x$  direction.

Our first objective is to use the available data to check the validity of the steady-state equations (2.18) and (2.19). These equations can be solved numerically to obtain  $|z|$  and  $\rho$  as functions of the growth parameters  $v$  and  $G$ ; but one needs the spacing  $\lambda_1$  in order to do this. Our results are shown in Table II where, for various values of  $v$ ,  $G$ , and  $\lambda_1$ , we list both the experimental and theoretical values of  $\rho$ . We also show the values of the ratio  $\lambda_1/l$  which, as argued previously, is a measure of the strength of the coupling between dendrites. All results shown here are for spacing  $W = 150 \mu\text{m}$ .

It is clear from this table that the agreement between experiment and theory is quite good at the higher growth rates where  $\lambda_1$  is greater than  $l$ . At slower speeds, however,  $\lambda_1$  is less than  $l$  and observed tip radii are appreciably larger than predicted. This trend is qualitatively consistent with the fact that, at the smallest speeds shown here, the system is undergoing a transition from a cellular pattern with relatively flat fronts and sharp grooves to the dendritic pattern with sharp paraboloidal tips and sidebranches.

We turn next to the stability theory summarized by Eqs. (2.32) and (2.33). The characteristic form of the eigenvalue  $\omega(\mathbf{q})$  is illustrated in Fig. 3. Here we have plot-

ted  $\omega$  as a function of  $q\lambda_1$ , in the interval  $-\pi \leq q\lambda_1 \leq \pi$ , for  $v = 20.0$ ,  $G = 67.0 \text{ K/cm}$ ,  $W = 150.0 \mu\text{m}$ , and three different values of  $\lambda_1$ . The system is clearly stable for  $\lambda_1 = 200.0 \mu\text{m}$ , unstable for  $\lambda_1 = 125.0 \mu\text{m}$ , and just neutrally stable for  $\lambda_1 = 166.529 \mu\text{m}$ . In every case that we have examined so far, the most dangerous mode, that is, the Fourier mode for which  $\omega(\mathbf{q})$  has an absolute maximum, occurs at the Brillouin-zone boundary  $q = \pm\pi/\lambda_1$ . In other words, the dominant instability is one in which every other dendrite grows at the expense of its nearest neighbors. The locus of points  $\lambda_1 = \lambda_0(v, G)$  for which  $\omega(\pi/\lambda_1) = 0$  is the neutral stability boundary in the space of variables  $v$ ,  $G$ ,  $\lambda_1$ .

Portions of our theoretical function  $\lambda_0(v, G)$  are shown in Figs. 4 and 5 along with the experimental data of Som-

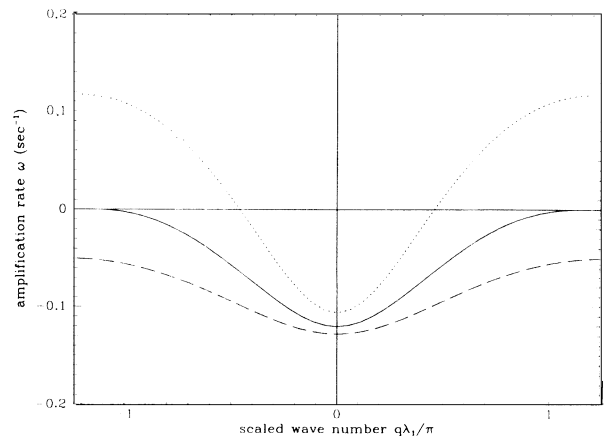


FIG. 3. Characteristic forms of the amplification rate  $\omega$  as a function of the scaled wave number  $q\lambda_1/\pi$ .

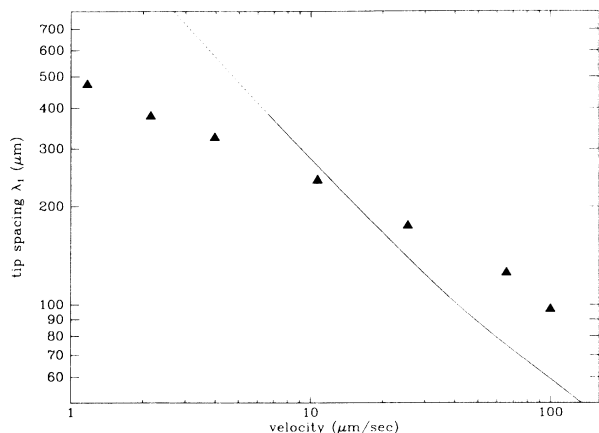


FIG. 4. Neutral stability curve  $\lambda_0$  as a function of growth velocity  $v$  for  $G=67.0$  K/cm and  $W=150.0$   $\mu\text{m}$ . The experimental points of Somboonsuk, Mason, and Trivedi (Ref. 9) are indicated by solid triangles.

boonsuk, Mason, and Trivedi<sup>9</sup> listed in Table II. The  $\lambda_1, v$  plane is shown in Fig. 4 for  $G=67.0$  K/cm, and  $W=150.0$   $\mu\text{m}$ . The function  $\lambda_0(v)$  is shown as a solid line for  $\lambda_0 > l$  and as a dotted line for  $\lambda_0 < l$ . We already know that our calculation is quantitatively incorrect for the latter case; here it appears to be qualitatively wrong in that it implies that the experimental points are on the unstable side of the stability boundary for slower growth speeds. What is more interesting, however, is that the experimental points are well inside the stable region at the higher speeds where we believe the calculation to be accurate. The  $G$  dependence of  $\lambda_0$  is shown in Fig. 5 for two different values of  $v$ . The fact that the distance between the experimental points and the stability boundary is very nearly insensitive to  $G$  is consistent with our expectation that the controlling variable is the ratio  $\lambda_1/l$ , which depends only on  $v$ .

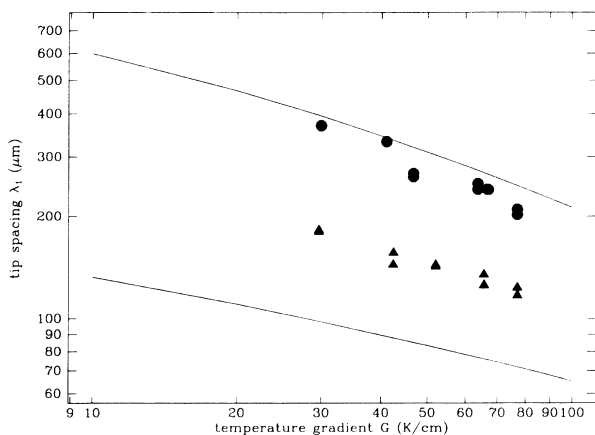


FIG. 5. Neutral stability curves  $\lambda_0$  as functions of temperature gradient  $G$  for two different growth speeds:  $v=10.7$   $\mu\text{m}/\text{sec}$  (upper curve) and  $v=65.0$   $\mu\text{m}/\text{sec}$  (lower curve). Experimental points are indicated, respectively, by circles and triangles.

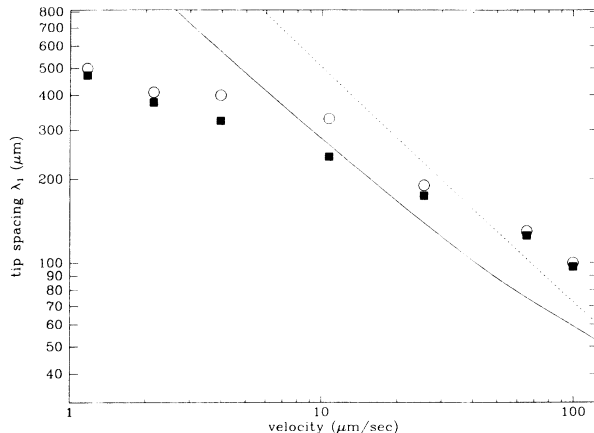


FIG. 6. Neutral stability curves for two different plate separations:  $W=50.0$   $\mu\text{m}$  (dashed curve) and  $W=150.0$   $\mu\text{m}$  (solid curve) for  $G=67.0$  K/cm. Experimental points are indicated, respectively, by open circles and solid squares.

Finally, it is interesting to note that our predicted variation of  $\lambda_0$  with spacing  $W$  seems qualitatively consistent with the observed variations of  $\lambda_1$ . In Fig. 6, we show  $\lambda_0$  as a function of  $v$  for  $W=50.0$  and  $150.0$   $\mu\text{m}$ , along with the corresponding experimental values of  $\lambda_1$ . Both the sign of the effect— $\lambda_1$  increases as  $W$  decreases—and its approximate magnitude are in agreement with theory.

#### IV. DISCUSSION

In summary, we find that our model of dendritic arrays seems sensible so long as the dendrites are coupled only weakly, that is, so long as the spacing  $\lambda_1$  is larger than the diffusion length  $l=2D/v$ . Under these conditions, the values of  $\lambda_1$  selected in the experiments of Somboonsuk, Mason, and Trivedi are well within the region of stability; no marginal stability mechanism seems to be operative.

These results suggest two important directions for further investigation. The first is experimental. It should be a relatively simple matter to determine the stability boundary experimentally by setting the system in motion as was done by Somboonsuk, Mason, Trivedi<sup>9</sup> and then reducing the pulling speed  $v$  in small steps until the instability occurs. This procedure would provide a quantitative test of our function  $\lambda_0(G, v)$  and, in a more fundamental sense, would check our argument about the existence of a continuous family of stable, steady-state patterns.

The second direction is theoretical. If the assumption of a continuous family of patterns can be verified as suggested in the previous paragraph, it becomes very important to understand how the observed patterns were actually achieved in the experiments. In this kind of situation, pattern selection must be history dependent. The ultimate value of  $\lambda_1$  chosen by the system must be determined by the way in which it is prepared initially, and by the sequence of pulling speeds which is imposed on it. A

theoretical description of these processes would require that the equations of motion derived here be generalized in such a way that  $\lambda_1$  becomes a dynamical variable. If such a generalization could be achieved, it would provide a crucial ingredient in numerical methods for simulating the formation of microstructures in the casting of alloys.

#### ACKNOWLEDGMENTS

This research was supported by U.S. Department of Energy Grant No. DE-FG03-84ER45108 and also in part by National Science Foundation Grant No. PHY82-17853, supplemented by funds from the National Aeronautics and Space Administration.

---

<sup>1</sup>W. Kurz and D. J. Fisher, *Fundamentals of Solidification* (Trans Tech, Switzerland, 1984).

<sup>2</sup>J. S. Langer, in *Chance and Matter*, Lectures on the Theory of Pattern Formation, Les Houches Summer School, Les Houches, 1986, edited by J. Souletie, J. Vannimenus, and R. Stora (North-Holland, New York, 1987), pp. 629-711.

<sup>3</sup>D. Kessler, J. Koplik, and H. Levine, *Adv. Phys.* **37**, 255 (1988).

<sup>4</sup>P. Pelcé, *Dynamics of Curved Fronts* (Academic, New York, 1988).

<sup>5</sup>W. Kurz and D. J. Fisher, *Acta Metall.* **29**, 11 (1981).

<sup>6</sup>J. D. Hunt, in *Solidification and Casting of Metals* (The Metals Society, London, 1979), p. 1.

<sup>7</sup>T. Dombre and V. Hakim, *Phys. Rev. A* **36**, 2811 (1987).

<sup>8</sup>M. Ben Amar and B. Moussallam, *Phys. Rev. Lett.* **60**, 317 (1988).

<sup>9</sup>K. Somboonsuk, J. T. Mason, and R. Trivedi, *Metall. Trans. A* **15A**, 967 (1984).

<sup>10</sup>J. S. Langer, *Rev. Mod. Phys.* **52**, 1 (1980).